

Thickness Dependent Magnetic and Dielectric Behavior of Iron Oxide Thin Films

Saira Riaz¹⁾, Aseyah Akbar²⁾, Shahid Atiq³⁾, *S. Sajjad Hussain⁴⁾
and Shahzad Naseem⁵⁾

1), 2), 3), 4), 5) *Centre of Excellence in Solid State Physics, University of the Punjab,
Lahore-54590, Pakistan*

⁵⁾ shahzad.cssp@pu.edu.pk

ABSTRACT

Thin iron oxide films have been a subject of many studies, primarily due to their interesting magnetic properties. These films can exhibit several crystal structures and compositions because of the different possible valence states of iron cations. These structures include wustite (FeO), which is a rocksalt phase, magnetite (Fe₃O₄), and maghemite (γ-Fe₂O₃), which are both cubic spinel phases, and hematite (α-Fe₂O₃), which is a corundum phase. Magnetite and maghemite have similar crystal structures, but the higher O/Fe ratio in the latter phase (i.e. maghemite) corresponds to a higher oxidation state of the iron ions. Iron oxide thin films are prepared using sol-gel and spin coating method. Thin films are deposited onto silicon substrates with variation in film thickness as 100nm, 200nm, 300nm, 400nm and 500nm. Thickness is confirmed using Variable Angle Spectroscopic Ellipsometer. These films are characterized using X-ray diffractometer (XRD), impedance analyzer and vibrating sample magnetometer (VSM). XRD patterns confirm the formation of phase pure magnetite. Crystallinity of the films increases as film thickness is increased to 400nm. With further increase in thickness crystallinity of the films decreases along with decrease in crystallite size. This increase in film thickness up to 400nm results in transition from weak ferromagnetic behavior to strong ferromagnetic behavior. Dielectric properties of iron oxide thin films show anomalous behavior whereas, normal dispersion behavior is observed in tangent loss. Highest dielectric constant and low tangent loss is observed for iron oxide thin films with 400nm thickness.

1. INTRODUCTION

Thin film has attracted worldwide attraction due to their unique properties that leads it wide applications as a catalyst and in spintronic devices (Alraddadi et al. 2016, Genuzio et al. 2016). The advantage that magnetic thin films offers over bulk materials includes size dependent magnetic as well as structural properties. Control of various parameters, including film thickness, leads to deviation in different properties thus making them suitable for diverse applications (Alraddadi et al. 2016, Genuzio et al. 2016, Motlagh and Araghi 2016).

Among various materials of interest magnetite is a potential candidate for various electronic and spintronic applications. In magnetite, both 2+ and 3+ states of iron cations are available. The magnetic moments linked to these cations are $5.0\mu_B$ and $4.0\mu_B$ (Nakamura et al. 2016, Tsuchiya et al. 2016, Craik 1975). No magnetization is linked to oxygen anions. The magnetic moments of Fe^{3+} cations cancel each other (Lai et al. 2006, Motlagh et al. 2016). Un-compensated magnetic moments lead to magnetization in Fe_3O_4 (Riaz et al. 2014a,b, Akbar et al. 2014a,b, Akbar et al. 2015).

Iron oxide thin films have diversity in their structure as well as magnetic properties. These properties can be tuned with variation in various parameters during deposition and /or preparation. The parameter varied in this research work is film thickness. Thickness is varied as 100-500nm.

2. EXPERIMENTAL DETAILS

Iron oxide films were prepared using spin method after synthesis of iron oxide sol. $Fe(NO_3)_3 \cdot 9H_2O$ was used as precursor. For sol synthesis, precursor was dissolved in suitable solvent and heated at $80^\circ C$ for sol synthesis (Riaz et al. 2014b, Akbar et al. 2014b).

Copper (Cu) was used as substrate. 5mmx5mm copper substrates were cleaned using acetone and isopropyl alcohol in ultrasonic bath for 15 minutes, separately (Asghar et al. 2006a,b). Thin films were coated on Cu substrates using Delta 6RC spin coater. During successive coatings, film was dried at room temperature. In this way number of coatings was varied in order to achieve required film thickness. Samples were named as S1-S5 with increase in number of coatings thereby, increasing film thickness.

For structural properties Bruker D8 Advance X-ray diffractometer (XRD), with $CuK\alpha$ (1.5406\AA) radiations, was used. Magnetic properties were studied with the help of Lakeshore's 7407 Vibrating Sample Magnetometer (VSM). Dielectric properties were studied with the help of 6500B Precision Impedance Analyzer.

3. RESULTS AND DISCUSSION

Thickness of the films was determined using "*M-2000 Variable Angle Spectroscopic Ellipsometer*". Model composed of three layers was built based on substrate material, film thickness and surface roughness. Film thickness and substrate roughness can be seen in Table 1. Decreases in roughness values was observed with increase in film thickness. This effect arises because of the availability of more nucleation sites with the increase in film thickness. Furthermore, probability of absorbed atoms increases with increase in thickness values thus producing more uniform layer after nucleation and by lowering energy difference between two nuclei. Therefore, the surface roughness decreases as film becomes more thick within the limitation of thickness. This effect is strengthened by XRD patterns. After saturation limit is achieved (in our case 400nm) the surface roughness increases.

Table 1 Film thickness and surface roughness for iron oxide thin films

Name	Film Thickness	Surface roughness
S1	100nm	3.5nm
S2	200nm	3.0nm
S3	300nm	2.8nm
S4	400nm	2.05nm
S5	500nm	2.58nm

XRD patterns for films S1-S5 can be seen in Fig. 1. Very small diffraction peaks of Fe_3O_4 phase were detected. Crystallinity of the films increases as film thickness was increased from 100nm to 400nm. With further increase in film thickness to 500nm decrease in crystalline order was observed. Lesser the film thickness, larger the number of grain boundaries per unit area. This leads to an increase in strain at low thickness values. The increase in film crystallite size with increase in film thickness resulted in reduction in grain boundaries that are present per unit area. So, a high extent of crystallization arises with increase in film thickness (Motlag et al. 2016, Lai et al. 2006).

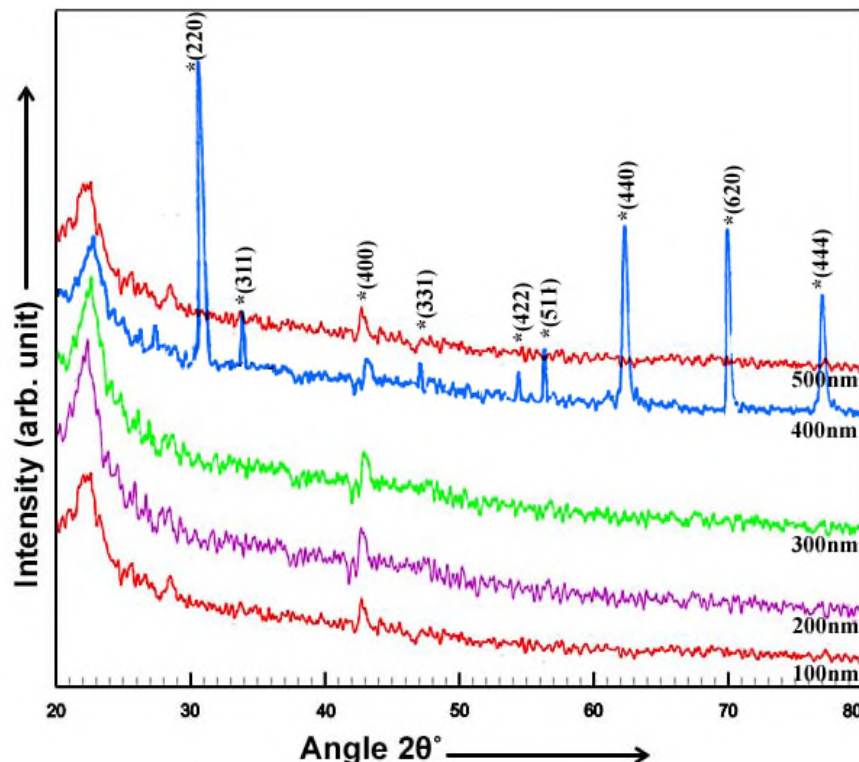


Fig. 1 XRD patterns for iron oxide thin films

Crystallite size (t), strain (Cullity 1956), dislocation density (δ) (Kumar et al. 2011) and lattice parameters (Cullity 1956) were calculated using Eqs. 1-4

$$t = \frac{0.9\lambda}{B \cos \theta} \quad (1)$$

$$\delta = \frac{1}{t^2} \quad (2)$$

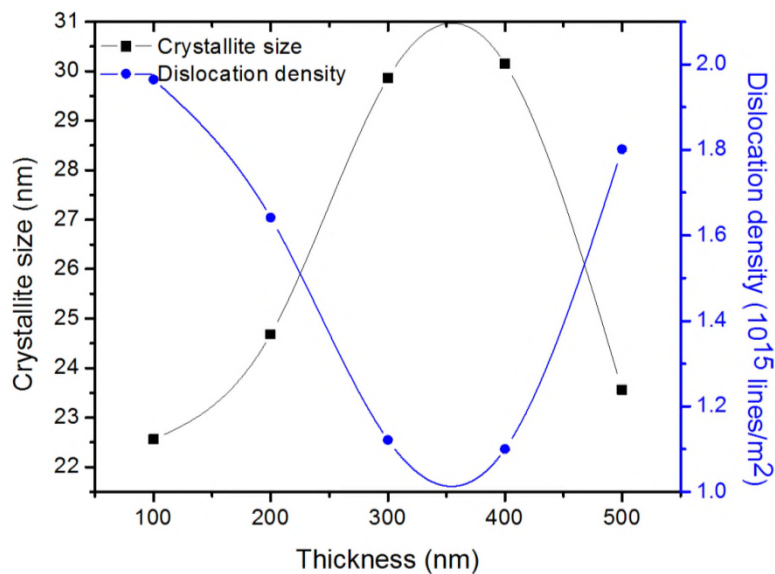
$$\text{Strain} = \frac{\Delta d}{d} = \frac{d_{\text{exp}} - d_{\text{hkl}}}{d_{\text{hkl}}} \quad (3)$$

$$\sin^2 \theta = \frac{\lambda^2}{4a^2} (h^2 + k^2 + l^2) \quad (4)$$

Where, θ is the diffraction angle, λ is the wavelength (1.5406Å) and B is Full Width at Half Maximum, d_{exp} is the d-spacing calculated using XRD patterns in Fig. 1 and d_{hkl} is the d-spacing taken JCPDS cards.

Crystallite size (Fig. 2) increases as film thickness was increased from 100nm to 400nm thus resulting in reduced strain and dislocation density. With increase in film thickness to 500nm decrease in crystallite size was observed. Lattice parameters and unit cell volume for iron oxide thin films listed in Table 2 are close to that reported in literature (Akbar et al. 2015).

Large numbers of grain boundaries are present in the films with low thickness (100nm) that leads to high strain value (Fig. 2(b)). As film thickness increases larger crystallites are formed thus resulting in decreased number of grain boundaries per unit area. It was also seen in Fig. 1 that films with thickness 400nm resulted in better crystallization as compared to other films indicating that number of defects that acts as trapping centre decreases. This fact is supported by decrease in strain at film thickness of 400nm. Beyond 400nm the defects including cracks, voids etc resulted in increase in dislocations and strain in iron oxide thin films (Motlagh et al. 2016).



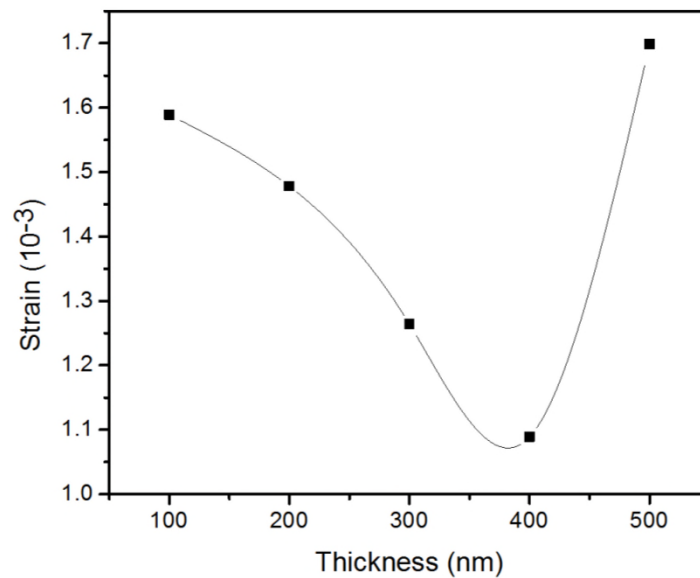


Fig. 2 Crystallite size, strain and dislocation density plotted as a function of film thickness

Table 2 Lattice parameters and unit cell volume for iron oxide thin films

Thickness (nm)	Lattice parameters (Å)	Unit cell volume (Å ³)
100	8.374	587.2173
200	8.370	586.3763
300	8.735	666.4825
400	8.370	586.3763
500	8.371	586.5864

M-H curves for iron oxide films can be seen in Fig. 3. Films with thickness 100-300nm showed weak magnetic behavior. Transition to strong ferromagnetic behavior was observed with increase in film thickness to 400nm. Magnetite (Fe₃O₄) is composed of Fe²⁺ and Fe³⁺ cations. These cations are arranged on octahedral and tetrahedral lattices. Fe²⁺ and Fe³⁺ have six and five electrons in their subshell, respectively. When these electrons are arranged, in accordance with Hund's rule, Fe³⁺ cations give high magnetic moment of 5.0μ_B as compared to Fe²⁺ cations. But these Fe³⁺ cations have antiferromagnetic coupling in the lattice. Therefore, magnetic moment of Fe²⁺ cations leads to net magnetization in Fe₃O₄ (Craik 1975, Riaz et al. 2014b, Akbar et al. 2015). This transition to ferromagnetic behavior is associated with transition in crystalline behavior of iron oxide films (Fig. 1).

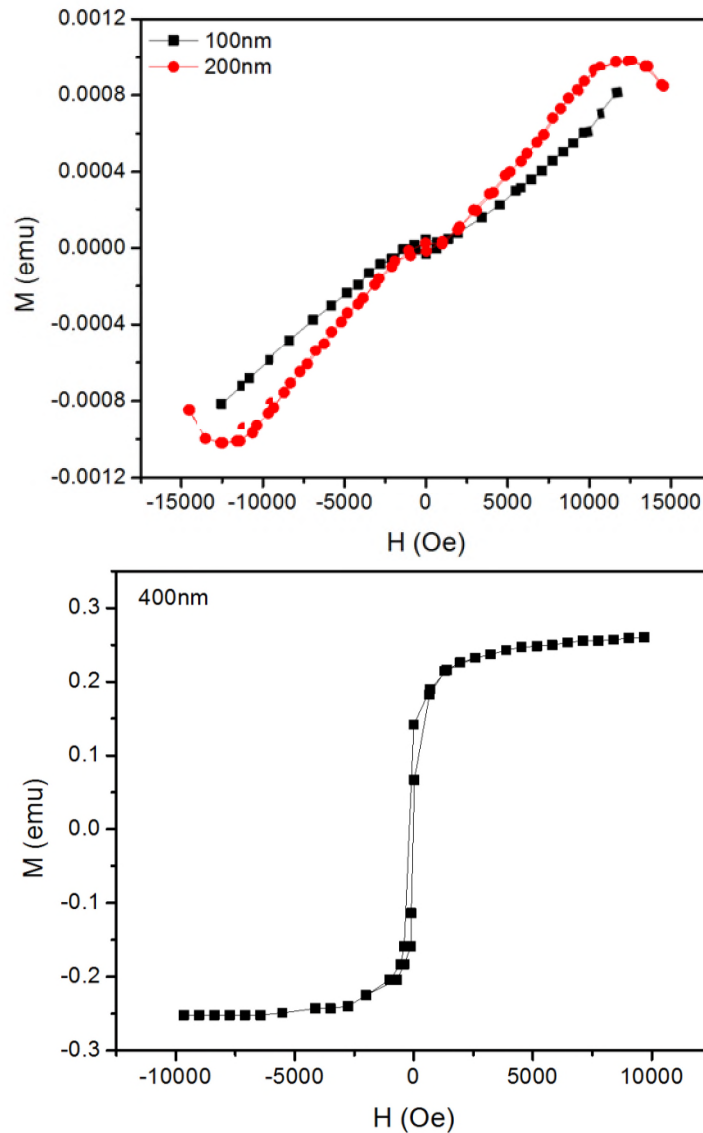


Fig. 3 M-H curves for iron oxide thin films

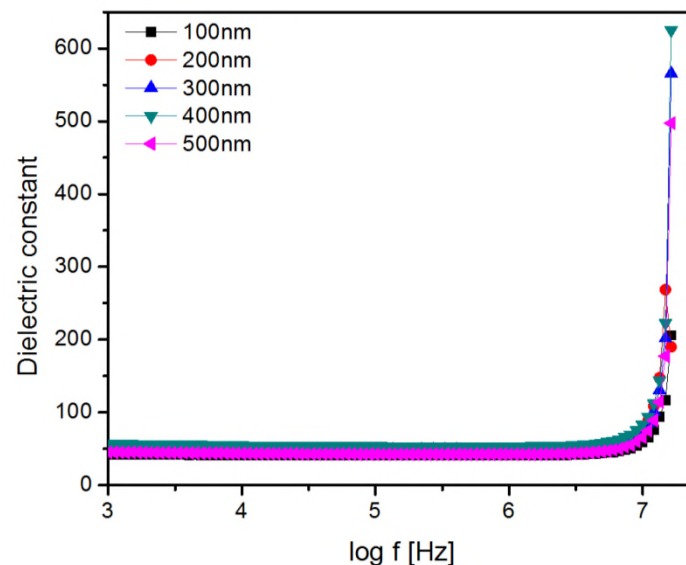
Frequency dependent capacitance and resistance was done using impedance analyzer and the dielectric constant and tangent loss were calculated using Eqs. 5 and 6 (Barsoukov and Macdonald 2005)

$$\varepsilon = \frac{C \times d}{\varepsilon_0 \times A} \quad (5)$$

$$\tan \delta = \frac{1}{2\pi f \varepsilon \varepsilon_0 \rho} \quad (6)$$

Where C is the capacitance in parallel plate configuration, d is the thickness of the specimen, A the area of the device, ε_0 is the permittivity of free space and ρ is the

resistivity. Tangent loss (Fig. 5) shows no anomaly in dispersion. This dispersion known as Debye type dispersion can be enlightened using Koop's theory. This theory is based on Maxwell-Wagner two layered Model. Based on this model there are grains and grain boundaries present in the specimen. Grains offer high conductivity and actively participate in high frequency region. This results in low dielectric constant at high frequencies. (Hu et al. 2011, Riaz et al. 2015). In thin films, because of reduced grain sizes grain boundaries play dominating role in dielectric studies. Due to reduced size, both grain and grain boundaries are larger in number as compared to that in bulk form. This makes polarization hard to comprehend (Riaz et al. 2015). On the other hand, dielectric constant shows anomalous behavior. This rise in dielectric constant at high frequencies is attributed to resonance effect. Resonance effect arises when frequency of externally applied electric field becomes equal to the jumping frequency of ions (Yang et al. 2010). This effect leads to increase in dielectric constant in high frequency region (Fig. 4(a)). Dielectric constant increases from 210 to 615 ($\log f = 7.3$) and tangent loss decreases as film thickness was increased to 400nm. This increase in dielectric constant is attributed to transition to crystalline structure as was observed in Fig. 1. This provides additional polarization ability to the dipoles thus increasing dielectric constant. In addition, as it was observed in Fig. 2 that strain decreases with increase in film thickness to 500nm. This is favorable for 180° domain structure. This also increases dielectric constant also (Riaz et al. 20156, Azam et al. 2015).



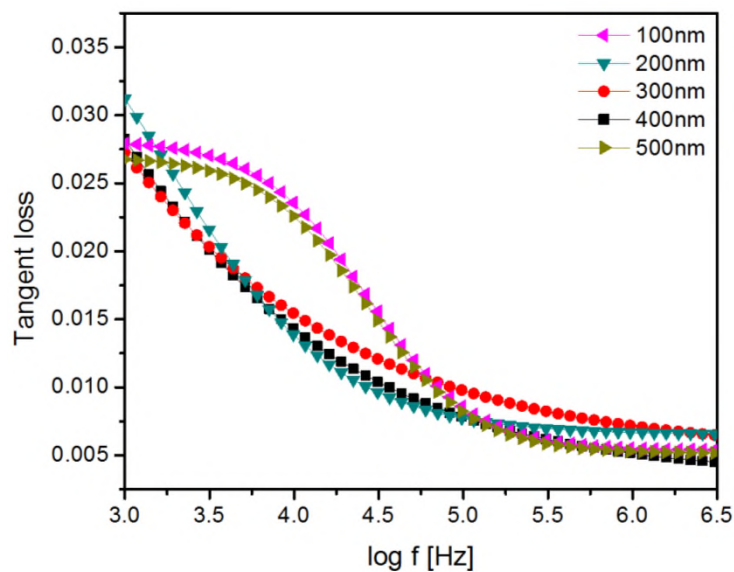


Fig. 5 Dielectric constant and tangent loss for iron oxide thin films

4. CONCLUSIONS

Iron oxide films were prepared using sol-gel method with variation in thickness as 100nm-500nm. Film thickness and surface roughness were determined using Variable Angle Spectroscopic Ellipsometer. XRD results showed transition from amorphous to crystalline behavior as thickness was increased from 100nm to 400nm. Further increase in film thickness to 500nm resulted in decrease in crystalline order in iron oxide films. Magnetization curves showed conversion from weak to strong magnetic behavior as thickness was increased to 400nm. Dielectric constant increases and tangent loss decreases as thickness was increased to 400nm. These results indicate that optimum thickness for iron oxide films is 400nm.

REFERENCES

- Akbar, A., Riaz, S., Ashraf, R. and Naseem, S. (2014a), "Magnetic and magnetization properties of Co-doped Fe_2O_3 thin films," *IEEE Trans. Magn.*, **50**, 2201204
- Akbar, A., Riaz, S., Bashir, M. and Naseem, S. (2014b), "Effect of $\text{Fe}^{3+}/\text{Fe}^{2+}$ ratio on superparamagnetic behavior of spin coated iron oxide thin films," *IEEE Trans. Magn.*, **50**, 2200804
- Alraddadi, S., Hines, W., Yilmaz, T., Gu, G.D. and Sinkovic, B. (2016), "Structural phase diagram for ultra-thin epitaxial $\text{Fe}_3\text{O}_4 / \text{MgO}(0\ 0\ 1)$ films: thickness and oxygen pressure dependence," *J. Phys.: Condens. Matter*, **28**, 115402
- Asghar, M.H., Placido, F. and Naseem, S. (2006(a)), "Characterization of reactively evaporated TiO_2 thin films as high and medium index layers for optical applications," *Eur. Phys. J. - Appl. Phys.*, **35**, 177-184.
- Asghar, M.H., Placido, F. and Naseem, S. (2006(b)), "Characterization of Ta_2O_5 thin films prepared by reactive evaporation," *Eur. Phys. J. - Appl. Phys.*, **36**, 119-124.

- Azam, M., Riaz, S., Akbar, A. and Naseem, S. (2015), "Structural, magnetic and dielectric properties of spinel $MgFe_2O_4$ by sol-gel route," *J. Sol-Gel Sci. Technol.*, **74**, 340–351
- Barsoukov, E. and Macdonald, J.R. (2005), "Impedance Spectroscopy Theory, Experiment, and Applications," John Wiley & Sons, Inc., Publication, New Jersey, 2005.
- Craik, D.J. (1975), *Magnetic Oxides*, John Wiley & Sons, New York.
- Cullity, B.D. (1956), "Elements of x-ray diffraction," Addison Wesley Publishing Company, USA.
- Genuzio, F., Schmidt, S.T., Menzel, D. and Freund, H.J. (2016), "Phase transformations in thin iron oxide films: Spectromicroscopic study of velocity and shape of the reaction fronts," *Surf. Sci.*, **648**, 177–187
- Hu, Y., Fei, L., Zhang, Y., Yuan, J., Wang, Y., Gu, H. (2011) "Synthesis of Bismuth Ferrite Nanoparticles via a Wet Chemical Route at Low Temperature," *J. Nanomater.* **2011**, 797639.
- Kumar, N., Sharma, V., Parihar, U., Sachdeva, R., Padha, N. and Panchal, C.J. (2011) "Structure, optical and electrical characterization of tin selenide thin films deposited at room temperature using thermal evaporation method," *J. Nano- Electron. Phys.*, **3**, 117-126
- Lai, F., Lin, L., Huang, Z., Gai, R. and Qu, Y. (2006), "Effect of thickness on the structure, morphology and optical properties of sputter deposited Nb_2O_5 films," *Appl. Surf. Sci.*, **253**, 1801–1805
- Motlagh, Z.A. and Araghi, M.E.A. (2016), "Effect of film thickness and texture morphology on the physical properties of lead sulfide thin films," *Semicond. Sci. Technol.*, **31**, 025017
- Nakamura, K., Kuriyama, N., Takagiwa, S., Sato, T. and Kushida, M. (2016), "Film fabrication of Fe or Fe_3O_4 nanoparticles mixed with palmitic acid for vertically aligned carbon nanotube growth using Langmuir-Blodgett technique," *Japanese J. Appl. Phys.*, **55**, 03DD06
- Riaz, S., Akbar, A. and Naseem, S. (2014a), "Ferromagnetic Effects in Cr-Doped Fe_2O_3 Thin Films," *IEEE Trans. Magn.*, **50**, 2200704
- Riaz, S., Ashraf, R., Akbar, A. and Naseem, S. (2014b), "Microwave Assisted Iron Oxide Nanoparticles—Structural and Magnetic Properties," *IEEE Trans. Magn.*, **50**, 2201504
- Riaz, S., Shah, S.M.H., Akbar, A., Atiq, S. and Naseem, S. (2015), "Effect of Mn doping on structural, dielectric and magnetic properties of $BiFeO_3$ thin films," *J. Sol-Gel Sci. Technol.* **74**, 310-319.
- Tsuchiya, T., Terabe, K., Ochi, M., Higuchi, T., Osada, M., Yamashita, Y., Ueda, S. and Aono, M. (2016), "In Situ Tuning of Magnetization and Magnetoresistance in Fe_3O_4 Thin Film Achieved with All-Solid-State Redox Device," *ACS Nano*, **10**, 1655–1661
- Yang, C., Jiang, J.S., Qian, F.Z., Jiang, D.M., Wang, C.M., Zhang, W.G. (2010), "Effect of Ba doping on magnetic and dielectric properties of nanocrystalline $BiFeO_3$ at room temperature," *J. Alloy Compd.*, **507**, 29–32.